Ultrasensitive detection of cancer biomarkers in serum by hybrid mechanical and optoplasmonic nanosensor

P.M. Kosaka, V. Pini, J.J. Ruz, R. A. da Silva, M. Ujue-González, D. Ramos, M. Calleja and J. Tamayo*

The blood contains a treasure trove of protein biomarkers, most of them still to discover, which will be crucial for early detection of disease and for personalized medicine[1-4]. A key point in this goal will be nanosensors capable of detecting with very high reproducibility biomarkers at concentrations of at least one million times lower than the rest of blood proteins[5-7]. In this letter, we propose a sandwich assay that involves the recognition of a protein cancer biomarker first by a surface-anchored antibody and second by an antibody free in solution that recognizes a free region of the captured biomarker. This second antibody is tethered to a gold nanoparticle that acts as mass and plasmonic label. The double signature is detected by means of a silicon cantilever that serves as mechanical resonator for 'weighing' the mass of the captured nanoparticles; and as optical cavity due to the two reflective opposite surfaces, that boosts the plasmonic signal from the nanoparticles. Merging mechanical and optical transduction schemes in the same platform provides remarkably superior performance and higher reliability than devices based on a single transduction scheme. The concept is demonstrated with two cancer biomarkers: the carcinoembryonic antigen (CEA) and the prostate specific antigen (PSA), currently in clinical use for diagnosis, monitoring and prognosis of colon cancer and prostate cancer, respectively[8]. A detection limit of 1×10^{-16} g ml^{-1} in serum is achieved with both biomarkers that is at least seven orders of magnitude better than in routine clinical practice[9]. More importantly, the rate of false positive and false negatives at this ultralow concentration is extremely low, $\approx 2 \times 10^{-4}$. The presented method is simple and affordable, and thus it can be implemented in health systems.

[1]Instituto de Microelectrónica de Madrid, CSIC, Isaac Newton 8 (PTM), Tres Cantos, Spain.
*e-mail: jtamayo@imm.cnm.csic.es

Protein composition in blood contains information from every cell in the body by either direct secretion to the blood stream or by intermediate signaling between neighboring cells. Refined proteomics technologies will increasingly provide reliable sets of protein biomarkers for each disease. Thus, among the most promising strategies for preventive cancer medicine is the detection of protein signatures that reflect the existence of the pathology from its initiation in some part of the body[1-4]. Protein biomarkers secreted by tumors at the very early stages, when symptoms are not developed and treatment is very effective, are at ultralow concentrations. Nanotechnology has provided biosensors with unprecedented levels of sensitivity that can be used for ultrasensitive monitoring of the biomarkers predicted by proteomics. However, nanosensors have also shown significant difficulties in issues regarding specificity and reproducibility, and hence they are still not ready for biomarker screening in blood[10-12]. One reason is the extreme difficulty in 'finding' low-abundance protein biomarkers in a 'haystack' of plasma proteins, some of them at concentrations at least 7 orders of magnitude higher (e.g., albumins~40 mg/mL). Thus, the situation is that the high biological noise set by the non-specific interactions largely exceeds the intrinsic noise of most of the nanosensors. In few words, the problem is not sensitivity; but i) specificity; to discriminate traces of biomarkers in the complex mixture of blood proteins, and ii) reliability, to minimize the painful false positives and false negatives in patient diagnosis. Therefore, our vision to translate nanosensors to the diagnosis arena involves: i) sandwich assays for enhancing specificity and signal amplification, and ii) detection of the biorecognition product by two transduction mechanisms for unequivocal diagnosis. The last, but not least important consideration is that the assay must be simple, i.e., no need of sophisticated instrumentation or new trained personal, as well as it must be affordable to be implemented in healthcare systems.

Here, we propose a sandwich assay that involves the recognition of a protein cancer biomarker first by a surface-anchored antibody and second by an antibody free in solution that recognizes a free region of the captured biomarker and is tethered to a 100-nm-diameter gold nanoparticle. The gold nanoparticle carries a significant mass, ≈10 fg, due to its size and high density (19 300 Kg/m^3), and exhibits localized plasmon resonances in the visible range of the electromagnetic spectrum consisting in a collective motion of free electrons. This phenomenon results in a resonant enhancement of the light absorption and scattering[13-14]. We choose silicon cantilevers for optomechanical detection of the gold nanoparticles that tag the sandwich assay. Cantilevers exhibit excellent mechanical attributes for their use as nanomechanical biosensors that translate biomolecular recognition on the cantilever surface into a number of nanomechanical signals that include quasistatic bending and resonant properties via a number of physical mechanisms such as biomolecular interactions, adsorbed mass, and stiffness of the biomolecules[15-24]. Here, we choose the dynamic-mode, in which the cantilevers oscillate at or near their resonance frequency, and this frequency decreases when gold nanoparticles land on the cantilever in linear proportion to the added mass. Here we demonstrate that microcantilevers can also exhibit enough structural quality to be used as optical resonators, i.e., the light can be efficiently transmitted or reflected through the cantilever for certain wavelengths via coherent internal reflection between the top and bottom interfaces of the microcantilever. Interestingly, biomolecular interactions on the cantilever surface modify the optical spectra of the cantilever. In particular, we harness this phenomenon for

detecting the plasmonic signature of the gold nanoparticles. Importantly, microcantilevers satisfy the requirements for availability and affordability as they are produced *en masse* by standard wafer-scale semiconductor processing techniques. Indeed, cantilevers with a large variety of geometries and mechanical responses are commercially available at reduced cost as a consequence of the expansion of the atomic force microscope (AFM).

The presented technology is challenged with the detection of ultralow concentrations of two cancer biomarkers spiked in undiluted serum, CEA (≈190 kDa) and PSA (≈32 kDa), currently in clinical use for diagnosis, prognosis and monitoring of colon and prostate cancers, respectively. The two biomarkers exhibit large differences in molecular weight and structure that allow to demonstrate the universality of the presented method. However, it is noteworthy to stress out that the biomarker concentrations analyzed here are at least three orders of magnitude lower than the cut-off concentrations used in clinical monitoring, and thus the presented technology does not add any advantage with respect to current technology for CEA and PSA blood tests. In fact, CEA and PSA as most of the current biomarkers suffer from low specificity for early disease detection. This work is addressed for the detection of low-abundance biomarkers secreted by the tumor at its early stage to the blood stream. It is expected that these biomarkers will be increasingly predicted with the hand of emerging proteomic tools[1-4].

A schematic of the sandwich assay is shown in Fig. 1a. The cantilevers and nanoparticles are respectively biofunctionalized with *capture antibodies* and *detection antibodies* by a procedure that ensures optimal recognition efficiency and ultralow fouling capability[12]. The materials and methods used in the functionalization and sandwich assays are detailed in the Supplementary Information (Section S1). The sandwich assay involves two biorecognition steps to enhance the selectivity and to amplify the sensor response. First, the functionalized cantilever is immersed in 1 mL of the fluid sample for one hour and 37°C to allow binding of the targeted biomarker to the *capture antibodies* immobilized on the cantilever surface. Second, after stringent rising of the cantilever to remove nonspecific adsorption, the cantilever is dipped in 1 mL of 1µg/mL solution of the *detection antibody* functionalized gold nanoparticles at 37°C for 1 hour.

A schematic of the mechanical detection of the sandwich bioassay is shown in Figs. 1c-1d. The materials and methods involved in the mechanical measurements are described in Supplementary Information (Section S2). We use commercially available arrays of silicon cantilevers, 500µm long, 100µm wide and 1 µm thick (Fig. 1b) that exhibit a fundamental resonance frequency of 5.08±0.18 kHz and a quality factor of 17.0±1.8 (statistics from 400 cantilevers). The resonance frequency is obtained from the driven vibration of the cantilever that is optically detected by means of the simple optical lever method[25] (Fig 1c). The cantilever array is driven by a piezoelectric actuator located beneath the chip base. The resonance frequency of the fundamental vibration mode of the cantilever is measured in air before and after the cantilever exposure to the gold nanoparticles functionalized with the detection

antibody. The mass loading gives rise to a decrease of the resonance frequency[20,26] (Fig. 1d). The intrinsic mass detection limit for these devices in air is of about 1 pg (10^{-12} g)[27], and thus the minimum detectable number of nanoparticles is ≈100. Although miniaturized nanomechanical resonators can detect in vacuum added masses of ~zg (10^{-21} g) or even smaller[27-29], we emphasize that this approach does not give any benefit here, as the biological floor noise due to non specific interactions in our experiments is ≈50 pg that corresponds to ~0.1 nanoparticles/μm^2. Advantageously, relatively large microcantilevers can be easily handled and measured with simple instrumentation. More importantly, diffusive transport sets a detection limit that scales up with the sensor area[11,17]. Indeed detection of ultralow concentrations of proteins with nanoscale sensors would require impractical long times, that in some cases it can achieve days.

A schematic of the optoplasmonic transduction of the captured biomarkers is shown in Fig. 2. In particular, we detect the enhanced light scattering of the gold nanoparticles due to their localized plasmon resonances (Fig. 2a), which makes that individual gold nanoparticles can be easily visualized through a dark-field microscope (Fig. 2b). Spectral analysis of the light scattered by a single biofunctionalized nanoparticle on silicon (Fig. 2c) reveals a peak at a wavelength of 620 nm with a linewidth of 88 nm, which provides the orange color to the nanoparticle in Fig. 2b. The fact that the gold nanoparticle is bounded to a silicon surface breaks the degeneration of the dipole plasmon modes, and thus the dipoles oriented parallel and perpendicular to the substrate display different optical resonance frequencies[30-32]. The observed scattering peak is a convolution of both dipole plasmon modes with a dominant contribution from the perpendicular dipole plasmon mode[32]. Figure 2d shows a scanning electron microscopy image of the cantilever region near the clamping that shows the 1 μm thick cantilever and 6 μm thick preclamping structure that is fixed to the chip (see Fig. 1b). The two opposite surfaces of the cantilever act as mirrors that enhance the light reflectivity for certain wavelengths in which constructive interference occurs between the multiple reflections from the two mirrors. Conversely, the reflectivity is suppressed for other wavelengths by destructive interference[33-34]. This is illustrated in the modulation of the reflectivity with the wavelength observed in cantilever with respect to the preclamping, where interference effects are negligible (Figs. 2e and 2f, Suppl. Sect. S2.3). As shown later on, when nanoparticles are bounded to the microcantilever, the optical cavity modes and the localized surface plasmon modes couple each other at very characteristic frequencies and form hybrid plasmonic supermodes[35]. This property is crucial for detecting ultralow concentrations of the cancer biomarker.

Once we have presented the basic physical elements of our biosensor, we analyze the mechanical and optical responses for ultralow concentrations of CEA and PSA that range from 10 ag/mL to 1 pg/mL in undiluted serum. For the sake of simplicity, we only describe in the main text the results for CEA, whereas the PSA results are summarized in Supplementary Materials, Section S5. The methodology used in the PSA detection assays is the same (Suppl. Information), and more importantly, the detection limits are very similar. The presented results comprise the response of 345 cantilevers for the CEA assays, and 334 for the PSA assays. None cantilever was discarded for the data analysis. To

discriminate the biorecognition signals from the non-specific interactions, we carried out for each detection assay, a stringent control experiment consisting in replacing the capture antibody by an antibody (anti-peroxidase antibody) no specific to CEA and using as a sample, a highly concentrated CEA solution (1µg/mL). The CEA detection antibody tethered to the gold nanoparticle was kept in the control assays. The assays were also performed in phosphate buffered saline solution (PBS), in addition to undiluted serum, to get insight on how the nonspecific binding of plasma proteins on the cantilever degrades the biosensor performance. Figure 3a illustrates the change of the resonance frequency peak of the cantilever induced by the nanoparticle recognition step for the control experiment (left) and for 1 pg/mL of CEA (right). Both experiments were carried out in PBS. In the control experiment, the resonance peaks before and after the nanoparticle recognition step are almost indistinguishable, whereas in the CEA detection assay, a significant shift of the resonance peak to lower frequencies is observed. The resonance frequency shift *versus* the CEA concentration is plotted in Fig. 3b for PBS (left) and undiluted serum (right) solutions. The noise floor levels due to non-specific interactions obtained from the control assays are also plotted. The assays were replicated at least 20 times for each concentration. The experimental data for PBS show an excellent agreement with the theoretical prediction based on the mass of the nanoparticles bound to the cantilever that we have quantified by thorough SEM inspection of the cantilevers (Supplementary Materials, Sections S2.5 and S3). The detection limits in these calibration curves are 0.1 fg/mL in buffer and one order of magnitude higher in serum, due to the huge amount of competing nonspecific interactions. The detection limit obtained in serum is six orders of magnitude better than that obtained by the benchmark technique in clinical diagnosis, enzyme-linked immunoabsorbent assay (ELISA), ≈1 ng/mL[9]. In the case of PSA, the detection limit in serum is also of about 1 fg/mL (Suppl. Sect. S5) that it is also significantly superior to ELISA, ≈10 pg/mL (Advia Centaur, Siemens).

Let us now switch to the plasmonic signal in the cantilever. Figure 4a shows the darkfield images of the cantilever near the preclamping region for a control experiment and for a detection experiment with 1 pg/mL of CEA in serum. The scattering signal is negligible in the control experiment. In the case of the CEA detection assay, a negligible increase of the scattering is observed in the preclamping region, whereas the cantilever region glows brightly. Further insight on this effect is obtained when the surface is inspected by a high-resolution darkfield objective (Fig. 4b). On the preclamping region, individual nanoparticles can be clearly distinguished at a surface density of about 1.2 μm^{-2}. In turn, the surface density of nanoparticles seems to be significantly higher on the cantilever region. We anticipate to the reader that SEM inspection shows no differences in the surface density of nanoparticles between the supporting chip, preclamping and the cantilever regions (Supplementary Information, Sections S2.5 and S3). To understand this effect, we make use of the schematics of the light/nanoparticle interaction shown in Fig. 4c. When the light interacts with a nanoparticle on either the cantilever preclamping or supporting chip, the scattered light is only collected in a solid angle given by the numerical aperture of the objective, referred to as backward scattering. When the nanoparticle is on the cantilever, in addition to the backward scattering, multiple pathways assist to enhance the scattering by a single nanoparticle. One pathway involves the amplification of the forward scattering by the

nanoparticle by multiple internal reflections. In this mechanism, the coupling between the dipolar plasmon resonance of the nanoparticle and the optical cantilever cavity resonances creates a hybrid mode that boost the scattering signal at the nanoparticle site[35]. In a second pathway, the refracted light undergoes multiple internal reflections in the optical cantilever cavity, resulting into a cascade of scattering interactions at the neighboring nanoparticle sites that leads to an apparent higher density of nanoparticles in the darkfield image. The scattering spectra of the zoomed regions in the preclamping and the cantilever are plotted in Fig. 4d (Suppl. Sect. S2.4). The coupling between the dipolar plasmonic modes and the individual modes of the cantilever microcavity leads to a twofold effect, first the plasmon-assisted scattering is enhanced by the optical cantilever cavity by almost one order of magnitude, and second, the nanoparticle plasmon spectra is discretized by the optical cavity modes of the cantilever[35].

The mean scattering signal obtained from the darkfield images is plotted in Fig. 5a as a function of the CEA concentration in serum (Suppl. Sect. S2.3). The hybrid plasmonic-microcavity mode plays a determining role for detecting ultralow concentrations of the cancer biomarker. Whereas the scattering signal in the preclamping for CEA concentrations below 1 pg/ml lies in the region obtained in the control experiments; strikingly, the scattering boosting by the cantilever optical cavity enables the discrimination of concentrations on the verge of 10 ag/ml, more than one order of magnitude better than that obtained from the measurement of the mechanical resonance frequency. A very similar behaviour is obtained in the case of PSA (Suppl. Sect. S5). We now analyze the reliability of the presented dual nanosensor. This is quantified by calculating the error rate, defined as the mean value of the false negative and false positive rates for each transduction mechanism and for a hybrid method[36] that uses an optimal linear combination of the scattering and mechanical resonance frequency shift signals (Fig. 5b). The methodology is described in the Supplementary Materials (Section S4). In general, the error rate is significantly smaller in the optoplasmonic transduction, below 10^{-3} for concentrations higher than 10 ag/mL. In the case of the nanomechanical transduction, the error rate decreases with the biomarker concentration from 0.3 at 10 ag/mL to 3x 10^{-3} at 1 pg/mL. The hybrid methods brings a moderate benefit for the lower concentrations, however, for concentrations higher than 1 fg/mL, the use of hybrid signal improves the confidence of the bioassay by almost one order of magnitude. The robustness of this dual biosensor leads to an extremely low error rate, below 3×10^{-4} for concentrations higher than 10 ag/mL.

We find that the scattering and mechanical signals show a narrow dynamic range, exhibiting a near flat dependence for concentrations higher than 10 fg/mL. This potential limitation is well justified by the extremely low detection limits, which can be used for determining the presence of rare biomarkers that would otherwise remain undetectable with the current techniques in clinical diagnosis[7]. The fast signal saturation suggests that the nanoparticle/nanoparticle and nanoparticle/surface interactions set a maximum surface density of nanoparticles. To confirm the above hypothesis, we have analyzed by SEM the nanoparticle distribution on the cantilever and preclamping/chip surfaces (Supplementary Material section S3). The nanoparticle distribution exhibits an intriguing behaviour. For the lowest

detectable concentration, 10 ag/mL, the nanoparticles preferably distribute as monomers, being about 80% of the total nanoparticles. Then as the biomarker concentration increases, the monomer surface density quickly achieves saturation, and the nanoparticles preferably form dimers on the surface. Similarly, as the biomarker concentration further increases, the surface density of nanoparticle dimers quickly saturates, and then the nanoparticles preferably form trimers on the surface. This fractal adsorption pattern[37] continues up to achieving saturation for concentrations higher than 100 fg/mL, in which a density of 1.25 nanoparticles per μm^2 is achieved with only 40% corresponding to monomers and the rest to clusters. Notice that this behaviour is not found in the control experiments, which clearly indicates that the extraordinary nanoparticle distribution found in the CEA assays is triggered by a few biomolecular recognition events on the cantilever surface. No differences were observed between the nanoparticle distribution in the chip, preclamping and cantilever. This behaviour is also found in PBS. Determining the underlying mechanisms that originates this distribution pattern possess a formidable challenge. Despite the complexity of the problem, it is clear that short-range and long-range interactions between the nanoparticles, the biomarker and the cantilever all play a favorable role in the amplification of extremely small amount of biorecognition events that surpass the detection limits predicted by simple considerations based on diffusion and convection transport[10-11].

In conclusion, we demonstrate that silicon cantilevers serve both for plasmonic and nanomechanical transduction of sandwich bioassays labeled with gold nanoparticles. With simple commercially available cantilevers and unsophisticated instrumentation, the presented technique enables the detection of ultralow concentrations of cancer biomarkers in blood. The use of two different transduction mechanisms in a single platform enables to determine the presence of a protein with extremely high statistical significance. All this attributes bring this hybrid mechanical and optoplasmonic device closer to the dream of early cancer detection in routine blood tests.

Acknowledgements

We acknowledge financial support from the Spanish Science Ministry (MINECO) through projects MAT2012-36197 and INMUNO-SWING ITP-2011-0821-010000; and from European Research Council through Starting Grant NANOFORCELLS (ERC-StG-2011-278860). The authors thank Dr. J.M. de la Fuente and Dr. V Grazu for their assistance on the biochemical functionalization protocols.

Author contributions

P.K., J.T & M.C. conceived and designed the work. P.K. and R.S. performed the bioassays. P.K. and V.P. carried out the mechanical and scattering detection. P.K., V.P. and J.T. developed the instrumentation for mechanical and plasmonics detection. P.K., M.U. and V.P. carried out spectral scattering measurements. D.R., V.P. and M.U. performed the spectra scattering modeling. V.P., J.R. and P.K. executed the SEM surfaces inspections and developed the software for the data treatment J.T., P.K and M.C. wrote this manuscript with inputs from all authors. All authors analyzed the data, discussed the results and commented on the manuscript.

Additional information

Supplementary information is available in the online version of the paper.

Competing financial interests: The authors declare no competing financial interests.

References

1 Liotta, L. A., Ferrari, M. & Petricoin, E. Clinical proteomics: written in blood. *Nature* **425**, 905-905 (2003).

2 Simpson, R. J., Bernhard, O. K., Greening, D. W. & Moritz, R. L. Proteomics-driven cancer biomarker discovery: looking to the future. *Current opinion in chemical biology* **12**, 72-77 (2008).

3 Hanash, S. M., Pitteri, S. J. & Faca, V. M. Mining the plasma proteome for cancer biomarkers. *Nature* **452**, 571-579 (2008).

4 Schiess, R., Wollscheid, B. & Aebersold, R. Targeted proteomic strategy for clinical biomarker discovery. *Molecular oncology* **3**, 33-44 (2009).

5 Stern, E. *et al.* Label-free biomarker detection from whole blood. *Nature nanotechnology* **5**, 138-142 (2009).

6 Swierczewska, M., Liu, G., Lee, S. & Chen, X. High-sensitivity nanosensors for biomarker detection. *Chemical Society reviews* **41**, 2641-2655 (2012).

7 de La Rica, R. & Stevens, M. M. Plasmonic ELISA for the ultrasensitive detection of disease biomarkers with the naked eye. *Nature nanotechnology* **7**, 821-824 (2012).

8 Kulasingam, V. & Diamandis, E. P. Strategies for discovering novel cancer biomarkers through utilization of emerging technologies. *Nature clinical practice Oncology* **5**, 588-599 (2008).

9 Zhou, F. *et al.* Sensitive sandwich ELISA based on a gold nanoparticle layer for cancer detection. *Analyst* **137**, 1779-1784 (2012).

10 Nair, P. & Alam, M. Performance limits of nanobiosensors. *Applied physics letters* **88**, 233120-233120-233123 (2006).

11 Squires, T. M., Messinger, R. J. & Manalis, S. R. Making it stick: convection, reaction and diffusion in surface-based biosensors. *Nature biotechnology* **26**, 417-426 (2008).

12 Kosaka, P. M. *et al.* Tackling reproducibility in microcantilever biosensors: a statistical approach for sensitive and specific end-point detection of immunoreactions. *Analyst* **138**, 863-872 (2013).

13 Mayer, K. M. & Hafner, J. H. Localized surface plasmon resonance sensors. *Chemical reviews* **111**, 3828-3857 (2011).

14 Anker, J. N. *et al.* Biosensing with plasmonic nanosensors. *Nature materials* **7**, 442-453 (2008).

15 Fritz, J. *et al.* Translating biomolecular recognition into nanomechanics. *Science* **288**, 316-318 (2000).

16 Braun, T. *et al.* Quantitative time-resolved measurement of membrane protein–ligand interactions using microcantilever array sensors. *Nature nanotechnology* **4**, 179-185 (2009).

17 Arlett, J., Myers, E. & Roukes, M. Comparative advantages of mechanical biosensors. *Nature nanotechnology* **6**, 203-215 (2011).

18 Boisen, A., Dohn, S., Keller, S. S., Schmid, S. & Tenje, M. Cantilever-like micromechanical sensors. *Reports on Progress in Physics* **74**, 036101 (2011).

19 Buchapudi, K. R., Huang, X., Yang, X., Ji, H.-F. & Thundat, T. Microcantilever biosensors for chemicals and bioorganisms. *Analyst* **136**, 1539-1556 (2011).

20 Tamayo, J., Kosaka, P. M., Ruz, J. J., San Paulo, A. & Calleja, M. Biosensors based on nanomechanical systems. *Chemical Society reviews* **42**, 1287-1311 (2013).

21 Longo, G. *et al.* Rapid detection of bacterial resistance to antibiotics using AFM cantilevers as nanomechanical sensors. *Nature nanotechnology* **8**, 522-526 (2013).

22 Huber, F., Lang, H., Backmann, N., Rimoldi, D. & Gerber, C. Direct detection of a BRAF mutation in total RNA from melanoma cells using cantilever arrays. *Nature nanotechnology* **8**, 125-129 (2013).

23 Thakur, G. *et al.* Investigation of pH-induced protein conformation changes by nanomechanical deflection. *Langmuir* (2014).

24 Ndieyira, J. *et al.* Surface stress sensors for rapid and ultrasensitive detection of active free drugs in human serum. *Nature nanotechnology* (2014).
25 Tamayo, J. *et al.* Imaging the surface stress and vibration modes of a microcantilever by laser beam deflection microscopy. *Nanotechnology* **23**, 315501 (2012).
26 Waggoner, P. S., Varshney, M. & Craighead, H. G. Detection of prostate specific antigen with nanomechanical resonators. *Lab on a chip* **9**, 3095-3099 (2009).
27 Ekinci, K., Yang, Y. & Roukes, M. Ultimate limits to inertial mass sensing based upon nanoelectromechanical systems. *Journal of applied physics* **95**, 2682-2689 (2004).
28 Hanay, M. *et al.* Single-protein nanomechanical mass spectrometry in real time. *Nature nanotechnology* **7**, 602-608 (2012).
29 Chaste, J. *et al.* A nanomechanical mass sensor with yoctogram resolution. *Nature nanotechnology* **7**, 301-304 (2012).
30 Knight, M. W., Wu, Y., Lassiter, J. B., Nordlander, P. & Halas, N. J. Substrates matter: influence of an adjacent dielectric on an individual plasmonic nanoparticle. *Nano letters* **9**, 2188-2192 (2009).
31 Fan, J. A. *et al.* Near-normal incidence dark-field microscopy: applications to nanoplasmonic spectroscopy. *Nano letters* **12**, 2817-2821 (2012).
32 Mock, J. J. *et al.* Distance-dependent plasmon resonant coupling between a gold nanoparticle and gold film. *Nano letters* **8**, 2245-2252 (2008).
33 Özkumur, E. *et al.* Label-free and dynamic detection of biomolecular interactions for high-throughput microarray applications. *Proceedings of the National Academy of Sciences* **105**, 7988-7992 (2008).
34 Gómez-Martínez, R. *et al.* Silicon chips detect intracellular pressure changes in living cells. *Nature nanotechnology* **8**, 517-521 (2013).
35 Schmidt, M. A., Lei, D. Y., Wondraczek, L., Nazabal, V. & Maier, S. A. Hybrid nanoparticle–microcavity-based plasmonic nanosensors with improved detection resolution and extended remote-sensing ability. *Nature communications* **3**, 1108 (2012).
36 Perkins, N. J., Schisterman, E. F. & Vexler, A. ROC curve inference for best linear combination of two biomarkers subject to limits of detection. *Biometrical Journal* **53**, 464-476 (2011).
37 Haerifar, M. & Azizian, S. Fractal-Like Kinetics for Adsorption on Heterogeneous Solid Surfaces. *The Journal of Physical Chemistry C* (2013).

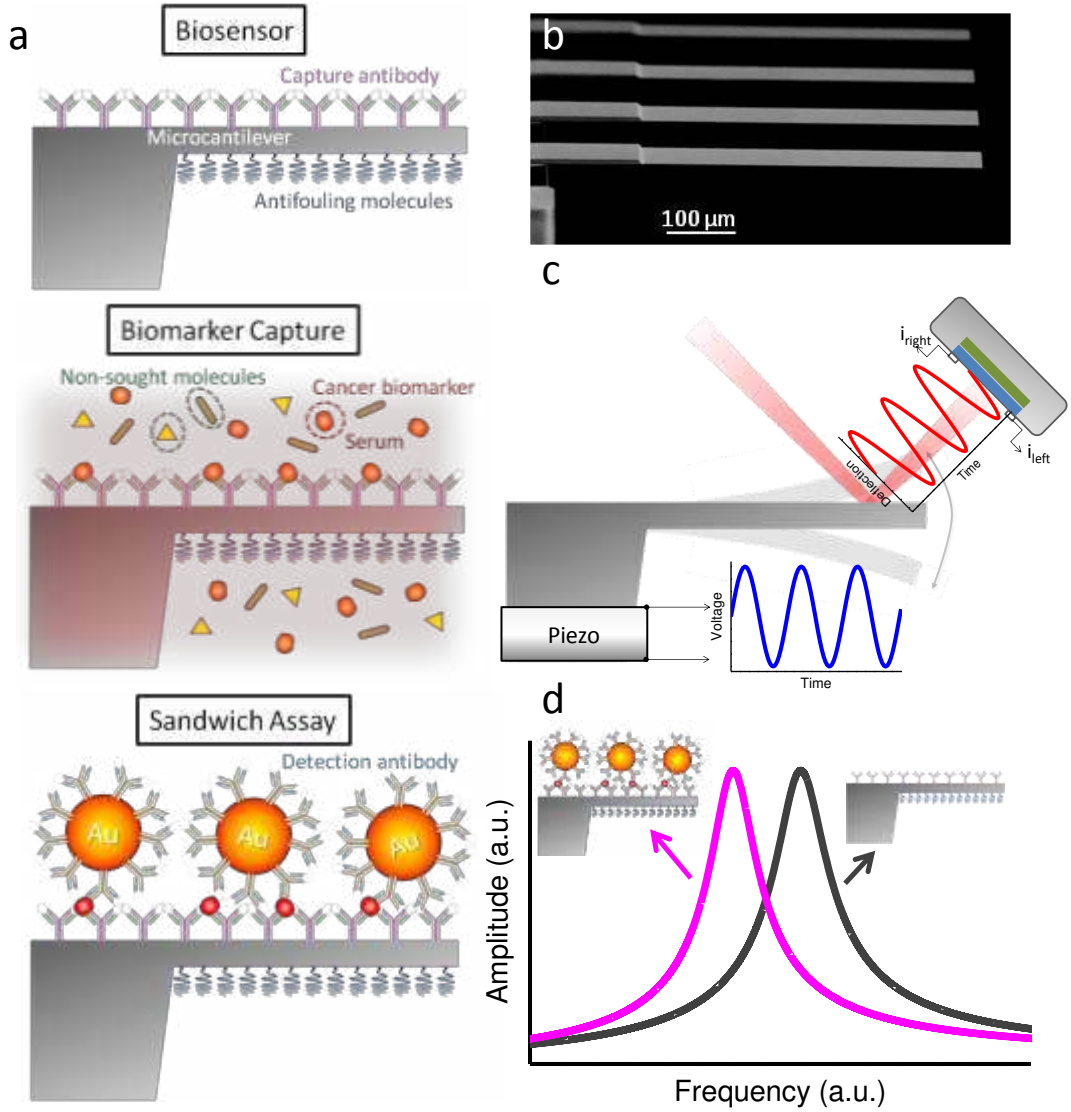

Figure 1 | Schematic representation of the sandwich assay on the cantilevers and its effect on the resonance frequency of the cantilever. **a,** The cantilever is functionalized with capture antibodies against the sought protein biomarker. The functionalization method comprises silanization, antibody binding on the top surface of the cantilever, and blocking with polyethylene glycol to minimize nonspecific interactions on the bottom surface of the cantilever and voids between the antibodies. The cantilever is then immersed in the serum sample to allow immunoreaction between the protein biomarker and the capture antibodies. Finally, the immunoreactions are revealed by exposing the cantilever to the detection antibodies against the biomarker that are tethered to 100-nm-diameter gold nanoparticles. The detection antibody recognizes a specific free region of the captured biomarker. **b,** Scanning electron microscopy image of the silicon cantilevers used in this work. The cantilevers are 500 µm long, 100 µm wide and 1 µm thick **c,** Schematics of the optical beam deflection method for measuring the cantilever vibration. A laser beam is focused onto the cantilever free end region. The deflection of the reflected beam due to the cantilever vibration is measured by a linear position-sensitive photodetector. The cantilever array is driven by a piezoelectric actuator located beneath the base. The vibration amplitude *versus* frequency is fitted to the harmonic oscillator model to derive the resonance frequency and quality factor of the cantilever. **d,** Schematics of the effect of the nanoparticle mass loading on the resonance frequency of the cantilever. The resulting downshift of the resonance frequency is proportional to the added mass.

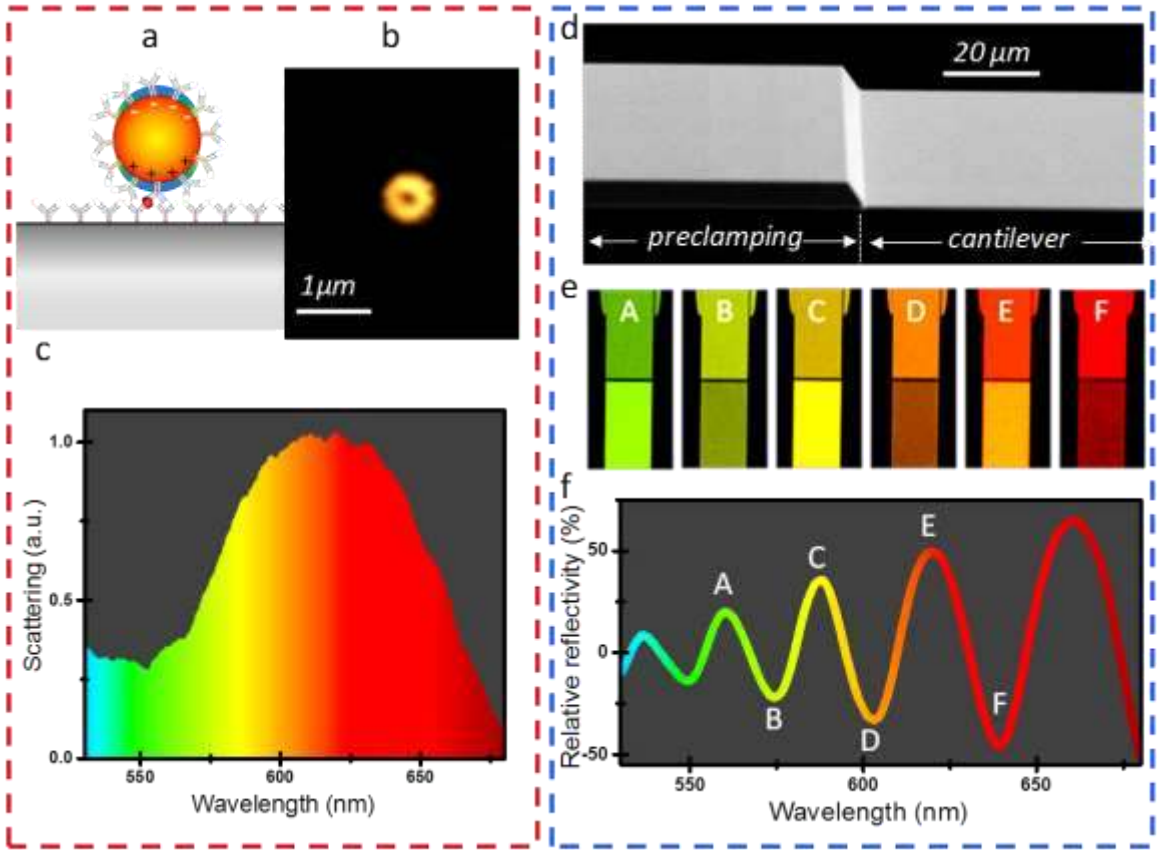

Figure 2 | Nanoparticle plasmon resonance and optical cantilever cavity. a, The gold nanoparticles used in the sandwich assay feature plasmon resonances associated with collective electron oscillations in the nanoparticle. These resonances give rise to enhanced scattering and absorption near the optical resonance frequency. **b,** Optical darkfield image of a single nanoparticle of 100 nm in diameter after performing a sandwich assay on a silicon substrate. The doughnut shape is related to the resonance plasmon dipole perpendicular to the surface that dominates the scattering. **c,** Scattering spectra collected from an area of 40 μm in diameter with a single nanoparticle. **d,** Scanning electron microscopy image of the cantilever clamping region that shows the frontier between the 6 μm thick preclamping structure fixed to the chip and the 1μm thick cantilever. **e,** Bright field images of the same cantilever clamping region at different illumination wavelengths in the visible region of the spectrum. The smaller thickness of the cantilever makes that the light can efficiently bounce multiple times between the opposite cantilever sides giving rise to an optical reflectivity enhancement at wavelengths in which constructive interference occurs and, conversely, to reflectivity suppression for wavelengths in which destructive interference occurs. The preclamping reflectivity modulation is negligible. **f,** Relative reflectivity in the cantilever with respect to the preclamping as a function of the wavelength. The caps letters label the wavelengths at which images in **e** were acquired.

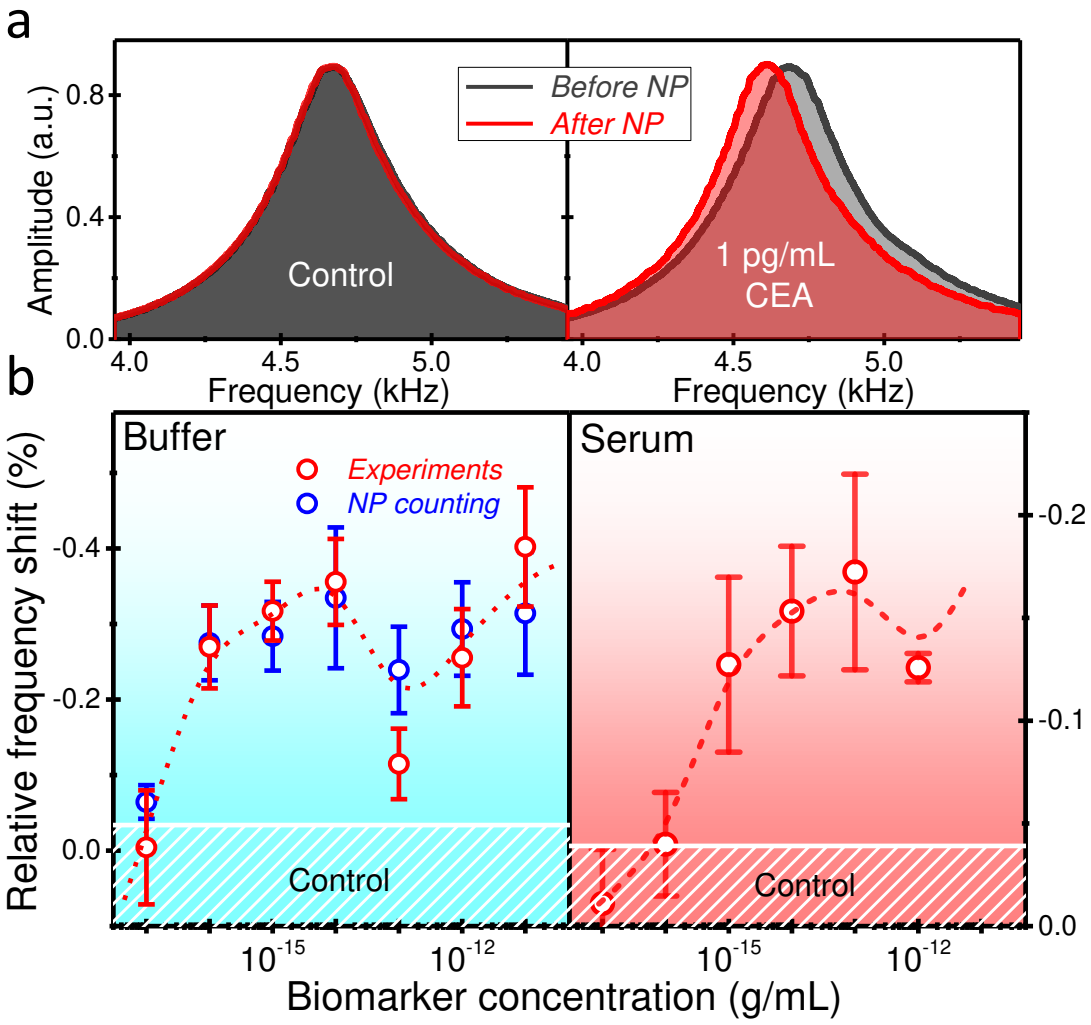

Figure 3 | Nanomechanical detection of the CEA protein biomarker. a, Mechanical resonance frequency of a silicon cantilever before and after the recognition step with the detection antibodies tethered to the gold nanoparticles for a control experiment and for a CEA detection assay (1 pg/ml in phosphate buffer saline). Measurements were carried out in air at room temperature. **b,** Relative resonance frequency shift of the fundamental vibration mode *versus* the biomarker concentration in buffer and sera samples (red symbols). The lines are a guide for the eyes. The frequency shifts measured in buffer solution are compared with the theoretical frequency shift predicted from the nanoparticle distribution on the cantilever obtained by scanning electron microscopy (blue symbols). The good agreement confirms that the frequency shift arises from the nanoparticle mass loading. The frequency shift for the control experiments is plotted as a dashed region that represents the mean value plus the standard deviation of the data.

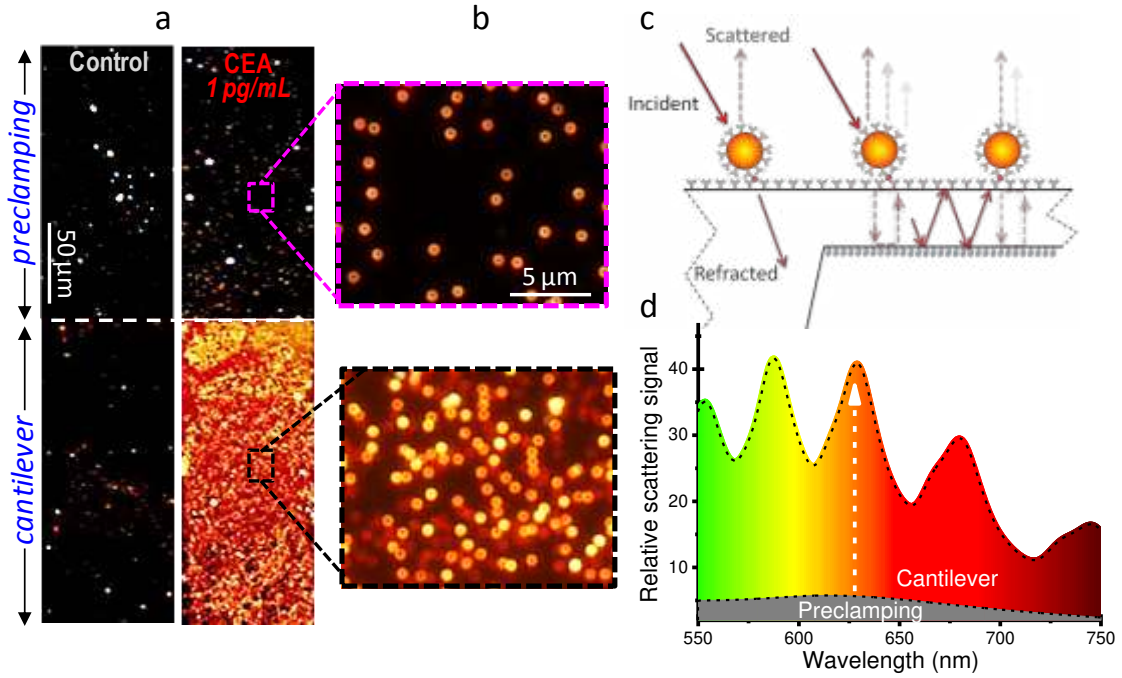

Figure 4 | Plasmonic detection of the CEA protein biomarker on the cantilever optical microcavity. a, Darkfield optical images of the cantilever after the recognition step with the antibodies tethered to the nanoparticles for a control experiment and for a CEA detection assay (1 pg/ml in serum). The scattering signal is negligible in the control experiment. In the case of the CEA detection assay, a negligible increase of the scattering is observed in the preclamping region, whereas the cantilever region glows brightly. **b,** High-resolution darkfield images of the preclamping and cantilever regions marked in **a**. In the preclamping region, individual nanoparticles can be clearly distinguished at a surface density of about 1.2 μm^{-2}. In the cantilever, it seems that the surface density of nanoparticles is significantly higher, although SEM inspection shows no differences in the actual surface density of nanoparticles between the preclamping and the cantilever regions. **c,** Schematics that illustrate the different pathways for generation of the darkfield signal in the cantilever via multiple internal reflections. **d,** Scattering spectra of the sandwich assay in the preclamping and cantilever regions for the CEA detection assay. The optical signal is the mean value from three regions of 40 µm in diameter. The scattering is normalized to that of a bare silicon chip. The coupling between the dipolar plasmonic modes and the individual modes of the cantilever microcavity leads to a twofold effect, first the plasmon-assisted scattering is enhanced by the optical cantilever cavity by almost one order of magnitude, and second, the nanoparticle plasmon spectra is discretized by the optical cavity modes of the cantilever.

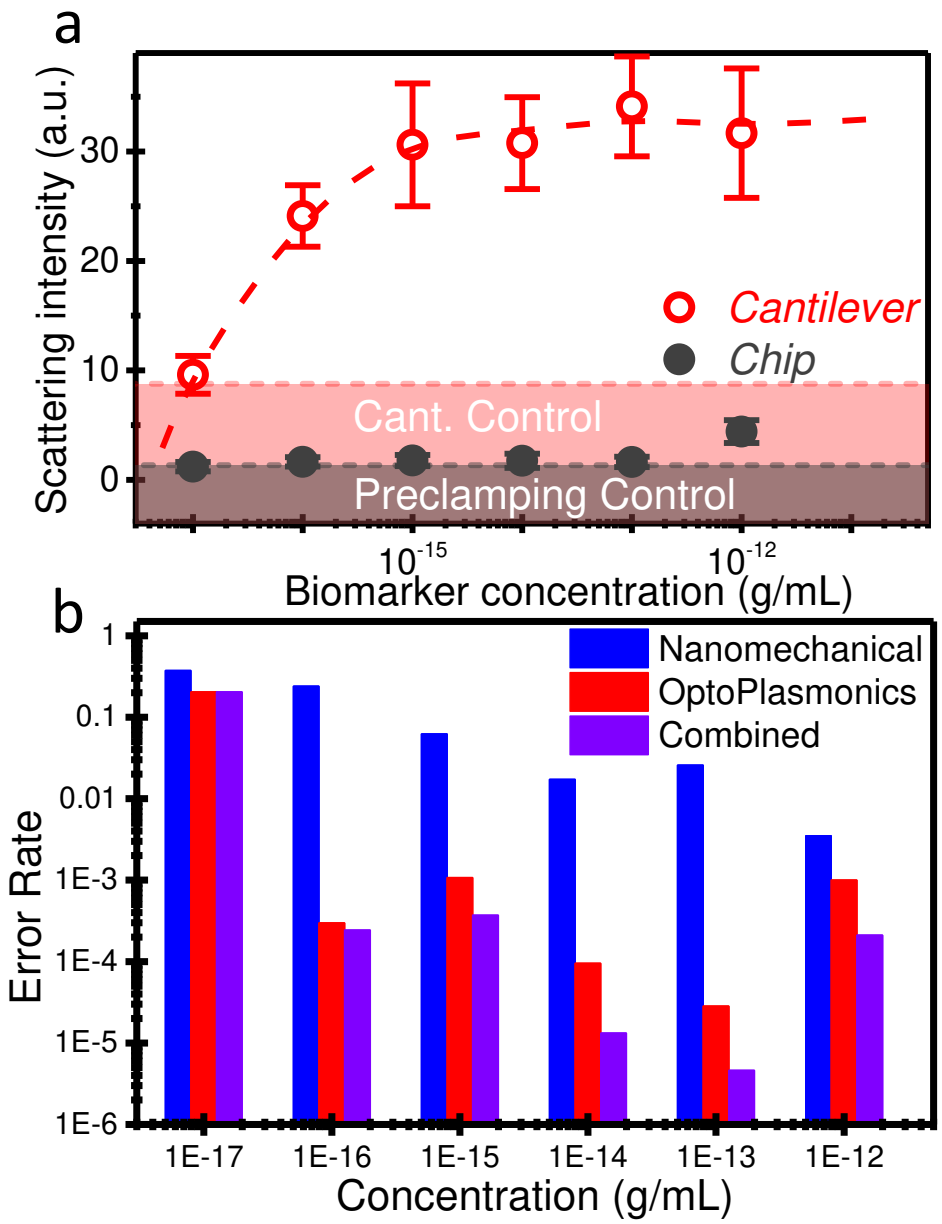

Figure 5 | Biomarker detection limit by unsophisticated plasmonic readout in cantilevers and reliability of the optomechanoplasmonic device. a, Mean scattering signal in the cantilever and the preclamping region *versus* the CEA concentration in serum. The signal is obtained from quick inspection of the cantilevers with a simple optical microscope and darkfield objective with low magnification. The data from the cantilever are compared with the data from the preclamping to assess the effect of the optical cantilever cavity. The scattering for the control experiments in the cantilever and preclamping regions are plotted as a dashed region that represents the mean value plus the standard deviation of the data. Whereas the scattering signal in the chip lies in the region obtained in the control experiments for CEA concentrations below 1 pg/ml, strikingly, the scattering boosting in the cantilever enables the discrimination of concentrations on the verge of 10 ag/ml. **b,** Error rate defined as the mean value of the false negative and positive rates as a function of the CEA concentrations for each transduction mechanism and for a hybrid method that uses an optimal linear combination of the scattering and mechanical resonance frequency shift signals.

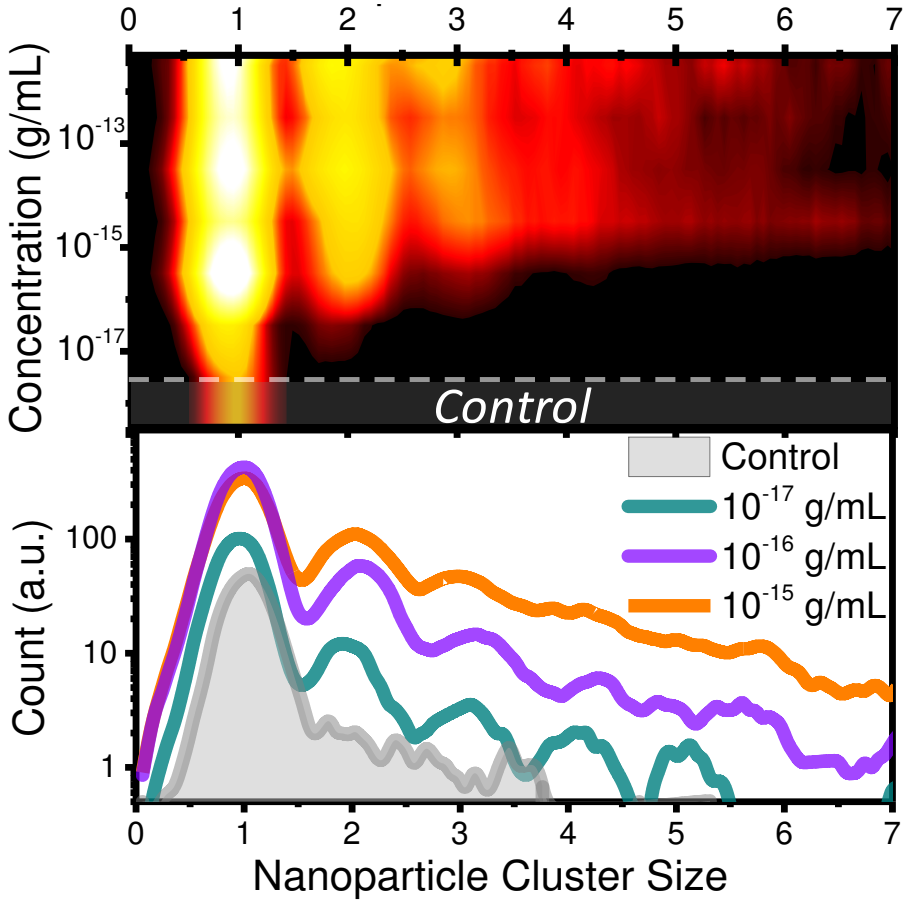

Figure 6 |Fractal nanoparticle distribution after the sandwich detection assay. Top: intensity color map of the nanoparticle distribution in clusters as a function of the concentration of the protein biomarker CEA. Bottom: Cross-sections of the intensity color map for the lower concentrations of CEA. The cluster distribution obtained in the control assays is also shown in both graphs.